New Insight into the Solid Electrolyte Interphase with Use of a Focused Ion Beam

Hong-Li Zhang, Feng Li, Chang Liu, Jun Tan, and Hui-Ming Cheng*

Shenyang National Laboratory for Materials Science, Institute of Metal Research, Chinese Academy of Sciences, 72 Wenhua Road, Shenyang 110016, China

Received: June 20, 2005; In Final Form: September 6, 2005

The formation and evolution of the solid electrolyte interphase (SEI) film on the surface of natural graphite spheres in the electrolyte of 1 M $LiPF_6$ in ethylene carbonate (EC) and dimethyl carbonate (DMC) (volume ratio 1:1) were investigated with use of focused ion beam (FIB) technology. Secondary electron FIB images clearly show the surface and cross-section morphology of the SEI film. The composition variation along the surface and cross section of the SEI film was also explored by the elemental line scan analysis (ELSA). The initial SEI film with an apparent thickness range of ∼450 to ∼980 nm is rough in morphology and nonuniform in composition, and contains small splits. After certain electrochemical cycles, the thickened SEI film displays microscale holes and obvious cracks on the surface, and the content of organic compounds increases. In addition, the concept of "internal SEI film" is first proposed based on the characterization of the cross section of the natural graphite spheres with the aid of FIB. Finally, the capacity fading mechanisms of the natural graphite spheres corresponding to different electrochemical stages are discussed.

Introduction

The model of solid electrolyte interphase (SEI), a kind of passivating layer that is conductive for ions but not for electrons, was first proposed by Peled[1] to describe the electrochemical behavior of alkali and alkaline earth metals in nonaqueous battery systems. With the rapid development of rechargeable lithium ion batteries (LIB), identification and characterization of the SEI film formed on various anodes becomes more and more important, since many of the performances of LIB, such as the first-cycle Coulombic efficiency (CE), irreversible capacity loss (ICL), and cycle life, are related to the formation and evolution of the SEI film.

So far, the structure, chemical composition, and morphology of the SEI film and its correlation with the electrochemical performance of LIB have been extensively studied.[2,3] Peled et al. proposed that the SEI film was a mosaic-type structure consisting of polyheteromicrophases,[4,5] where inorganic compounds may predominate in the inner part and organic compounds are usually formed in the outer part,[3] and applied X-ray photoelectron spectroscopy (XPS) and time-of-flight secondary-ion mass spectrometry (TOF-SIMS) to carefully analyze the SEI film formed on the basal and edge planes of highly ordered pyrolytic graphite (HOPG).[6−8] They found that there were obvious differences in the composition and thickness for the SEI films on the different planes, and deduced that solvents were preferentially reduced on the basal plane and the salt anions on the edge plane. Aurbach et al.[9−18] used XPS, Fourier transform infrared spectroscopy (FTIR), scanning electron microscopy (SEM), energy dispersive analysis by X-ray (EDAX), X-ray diffraction (XRD), and electrochemical impendence spectroscopy (EIS) etc. to systematically investigate the SEI film in different electrolytes and on different electrode surfaces. They concluded that the surface chemistry on the graphite electrode was similar to that on lithium metal in the same electrolyte, and the species included in the film were mainly Li_2O, Li_2CO_3, LiOH, $ROCO_2Li$, ROLi, LiX (X = F, Cl, etc.), and Li_xMF_y (M = P, As, etc.) depending on salts and solvents, among which Li_2CO_3 was one of the best passivating agents. Inaba and Ogumi et al. explored the topographical changes of the basal plane of HOPG in several electrolytes by scanning tunneling microscopy (STM)[19,20] and atomic force microscopy (AFM),[21,22] and noted a large swelling with a "hill-like" or "blister" feature on the plane in the initial stage of SEI formation in ethylene carbonate (EC)-based solutions. They attributed the phenomenon to solvent co-intercalation into graphite, which was proposed by Besenhard et al.[23,24] Dahn et al. claimed that the SEI film dramatically slows the kinetics of electrolyte decomposition by forming a physical barrier between the lithiated carbon electrode and electrolyte.[25] In addition, synchrotron radiation photoelectron spectroscopy (SRPS),[26] surface enhanced Raman scattering (SERS),[27,28] and transmission electron microscopy (TEM)[29,30] were also used to characterize the SEI film.

Although much information about the SEI film has been acquired by various spectroscopic, surface analytical, and electrochemical techniques mentioned above, efforts aimed at developing new characterization tools, as noted by Tarascon and Armand,[31] must be vigorously pursued so as to create a comprehensive database on the electrode−electrolyte interface. Furthermore, many of the above-mentioned techniques do not give information inside anode materials. In this study, we first applied focused ion beam (FIB) technology, on one hand, to investigate the evolution of morphology and composition of the SEI film upon repeated cycling formed on the surface of natural graphite spheres in the electrolyte of 1 M $LiPF_6$ in ethylene carbonate (EC) and dimethyl carbonate (DMC) (volume ratio 1:1). On the other hand, the formation of the SEI film around cracks inside the natural graphite spheres was found with the aid of FIB, and the concept of "internal SEI film" was proposed. Finally, based on the evolution of the SEI film, capacity fading mechanisms of natural graphite spheres at different electrochemical stages were discussed.

* Address correspondence to this author. Fax: 86-24-2390-3126. E-mail: cheng@imr.ac.cn.

10.1021/jp053311a CCC: $30.25
Published on Web 11/05/2005

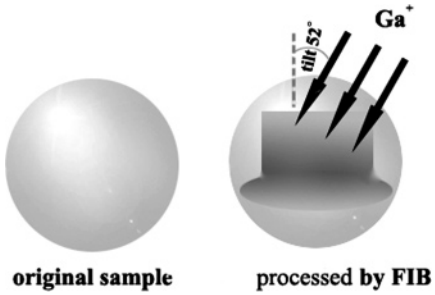

Figure 1. A schematic diagram showing the FIB processing to obtain the cross section of a natural graphite sphere.

Experimental Section

An electrochemical cell was assembled in an Ar-filled glovebox (Mbraun, Unilab, H_2O and O_2 <1 ppm) with a working electrode composed of natural graphite spheres (85 wt %, from Qingdao, China) whose average diameter is ~20 μm, BET surface area 4.3 m^2/g, BJH adsorption average pore size 21.4 nm and cumulative pore volume 0.025 cm^3/g, carbon black (5 wt %) and poly(vinylidene fluoride) (PVDF) binder (10 wt %), a lithium foil counter electrode, and a porous separator (Celgard 2400). The electrolyte was 1 M $LiPF_6$ in a mixture of EC/DMC (1:1 volume ratio) (battery grade, from Beijing Phylion Battery Company, with a content of water less than 10 ppm). To investigate the freshly formed SEI film on the surface of the natural graphite spheres, the cell was discharged (intercalation of lithium ions into graphite) to 0 V from open-circuit voltage (OCV). To discuss the evolution of the SEI film, the cell was galvanostatically charged and discharged in the voltage range of 0.001−2.5 V versus Li/Li^+ at a current density of 0.2 mA/cm^2 for 5 cycles and 24 cycles, respectively.

A FIB workstation using a liquid metal ion source to generate ions (typically Ga^+) to sputter specimens mainly performs three functions: generating ion images, removing material, and depositing material. An especially attractive feature of the FIB technique is its ability to accurately cut a specimen at any user-defined site in a short time, thus providing an opportunity of obtaining a cross section for studying various interfacial phenomena in a heterogeneous microstructure.[32−34] Herein, the working electrode after reaching preset charge/discharge states was treated as follows for the FIB (Nova 200, Nanolab) characterization: It was taken out of the cell in the Ar-filled glovebox, and washed with DMC solution. Afterward, it was heated in a vacuum at 60 °C to remove the residual DMC, and then transferred into the vacuum chamber of the FIB instrument in a sealed container. Figure 1 shows the schematic diagram of processing the sample by FIB, in which Ga^+ was accelerated at a high voltage (typically 30 kV) to sputter the natural graphite sphere scraped from the working electrode. Thereby, a cross section of the natural graphite sphere with a tilted angle of 52° relative to the ion sputtering direction was obtained.

Results and Discussion

An SEM image of a typical original natural graphite sphere is shown in Figure 2a. It can be seen that there are many cracks and flakes on the surface, which may exfoliate easily during intercalation/deintercalation of Li^+. Panels b−d of Figure 2 present the secondary electron FIB images and corresponding elemental line scan analysis (ELSA) curves of a treated natural

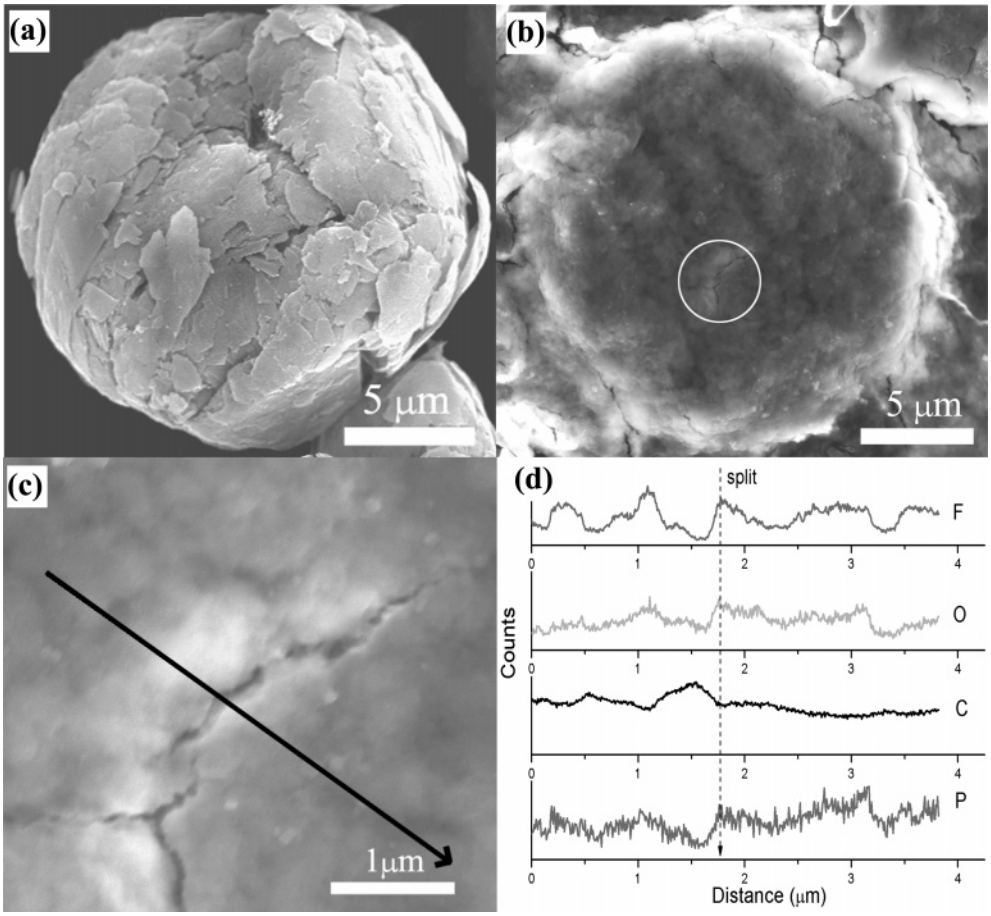

Figure 2. (a) SEM image of an original natural graphite sphere. (b) A secondary electron FIB image of the natural graphite sphere discharged to 0 V from OCV. (c) The magnified image of the circle area in panel b. (d) The elemental line scan analysis curves along the black line in panel c.

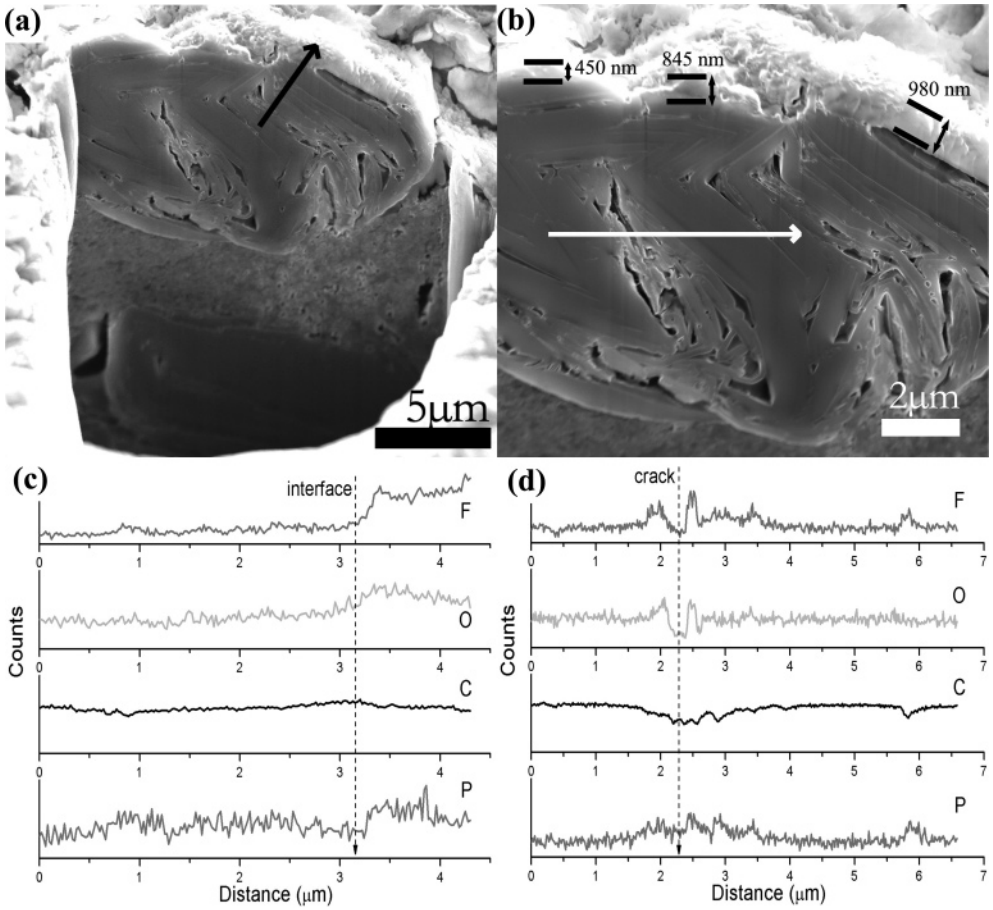

Figure 3. (a and b) Secondary electron FIB images of the cross section of a natural graphite sphere shown in Figure 2b. (c and d) The elemental line scan analysis along the black and white lines in panels a and b, respectively.

graphite sphere from a working electrode discharged to 0 V from OCV. A rough film formed on the surface of the natural graphite sphere can be obviously discerned in Figure 2b, which shields the original surface cracks as shown in Figure 2a. Moreover, a small split (Figure 2c) in the film is also observed possibly due to the increase of internal pressure from gas production causing the expansion of the graphite sphere, which will be proved later. The ELSA curves in Figure 2d indicate the relative content variation of fluorine (F), oxygen (O), carbon (C), and phosphorus (P) along the black line in Figure 2c. On the basis of the solvents, salt, and binder used here, the possible sources of these elements are analyzed as follows:[15,16] F is from $LiPF_6$, Li_xPF_y, LiF, and PVDF; O is from Li-alkyl carbonates (CH_3OCO_2Li, $(CH_2OCO_2Li)_2$, etc.), CH_3OLi, Li_2CO_3, LiOH, and Li_2O; C is from Li-alkyl carbonates, CH_3OLi, Li_2CO_3, and graphite spheres; P is from $LiPF_6$ and Li_xPF_y. We note that the contents of F, O, and P show a similar changing tendency, which is reversed for C (Figure 2d). According to the alternate variation of peaks and valleys in the ELSA curves, it can be concluded that the surface species of the freshly formed SEI film are distributed non-uniformly, which is due to different reactivity toward electrolytes on different local parts (type of crystallographic plane, ratio of basal to edge planes, etc.) of the natural graphite spheres.

Figure 3 shows the cross section of the natural graphite sphere shown in Figure 2b and the related ELSA curves. It can be seen that a very flat cross section, which is difficult to achieve with conventional processing methods since it is hard to accurately cut samples of ~20 μm, was obtained with the aid of FIB. The existence of the SEI film is clearly identified according to the contrast difference through the cross-section images, which also make the direct measurement of the SEI film thickness achievable. So far, there is no general conclusion about the thickness of the SEI film. Kong et al.[35] reported a 36 nm thick SEI film on the surface of HOPG by using ellipsometric spectra; Yazami[36] observed a 200 nm thick film on the surface of lithiated graphite fiber by SEM; Dahn et al.[25] calculated a SEI thickness of 45 ± 5 Å on the carbon particles; Peled et al.[2] obtained the depth profile of the SEI formed on the basal and edge plane of HOPG by controlling the sputtering time of XPS and got a rough estimate of the SEI thickness: 7 nm for basal SEI and 35 nm for edge SEI. The reason for this obvious difference in thickness from each report is partly due to the difficulties in its direct observation, and also related to what kind of electroactive materials, electrolytes, and electrochemical states are chosen in respective studies. Here, on the basis of both the contrast differences and element variations in ELSA curves, we measure from the cross section that the apparent thickness of the SEI film is in the range of ~450 to ~980 nm as shown in Figure 3b. The large variation in thickness is because of the unique surface features of natural graphite spheres, on which there are both basal and edge planes and many cracks (see Figure 2a). And just the feature diversity influences the surface catalytic properties and then the formation of the SEI film.[3] In addition, the observation of the internal texture of the graphite sphere is also achieved by the cross-section images, where many cracks with a width of hundreds of nanometers are found. More importantly, we observe evidence that electrolyte is decomposed around the internal cracks according to the ELSA result that will be discussed later. In other words, the SEI film can be formed not only on the outer surface but also along the internal cracks of the natural graphite sphere.

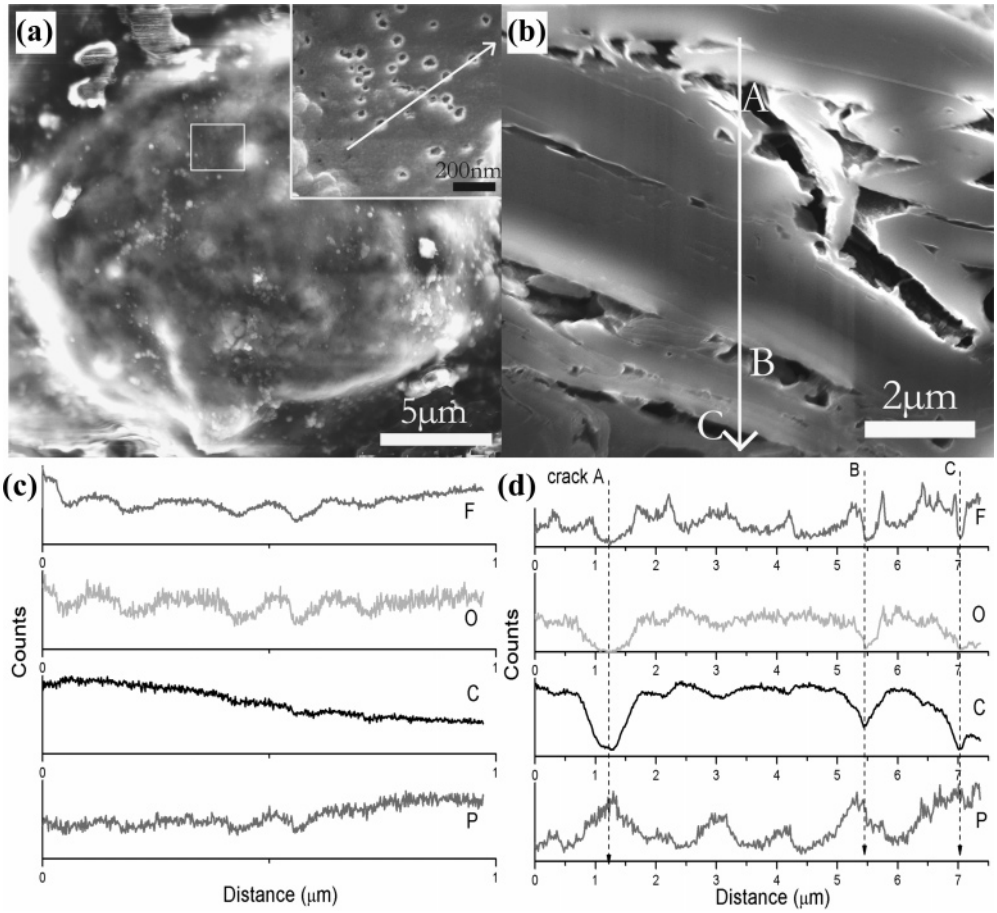

Figure 4. (a) A secondary electron FIB image of the natural graphite sphere after 5 electrochemical cycles; the inset shows the magnified image of the rectangle. (b) The internal cross-section image of the graphite sphere. (c and d) The elemental line scan analysis along the white lines in panels a and b, respectively.

This may be reasonably explained since electrolyte solutions can diffuse into the inside of the natural graphite spheres through surface cracks and accumulate in the internal cracks and then decompose to form the "internal SEI film", which also consumes a large amount of irreversible lithium ions and thus is responsible for the capacity fading of the natural graphite spheres. Figure 3c presents corresponding ELSA curves along the black line in Figure 3a. It can be seen that the contents of F, O, and P change remarkably through the film, whereas the relative content of C remains nearly unchanged. This is because, on one hand, the freshly formed SEI film is mainly comprised of fluorides such as LiF, a small amount of Li-alkyl carbonates (CH_3OCO_2Li, $(CH_2OCO_2Li)_2$, etc.) from the decomposition of EC/DMC, and a few species containing phosphorus (e.g., Li_xPF_y); on the other hand, the thick SEI film may be formed just in the surface cracks of the natural graphite sphere, into which electrolyte solutions penetrate reaching a certain depth and decompose there. That is, reduction products of electrolytes are actually embedded in the surface cracks. Therefore, the scanning signal of element C is from both the bulk and the surface of the natural graphite sphere, showing nearly no variations in the whole range; the apparent thickness (~450 to ~980 nm) of the embedded SEI film is unusual compared with other results. In fact, the intrinsic thickness of an initial SEI film, we believe, cannot reach values such as those above. Figure 3d shows the ELSA curves along the white line in Figure 3b. On the left and right sides of the crack, distinct peaks of F and O are shown and their intensities of recorded counts in the scanning process are similar to that of F and O plateaus in the outer SEI film (shown in Figure 3c), indicating that the "internal SEI film" with a thickness of several hundreds of nanometers has been formed around the crack and its composition is similar to that of the SEI film formed freshly on the graphite sphere surface.

To investigate the evolution of the SEI film, a natural graphite sphere from the working electrode after five discharge/charge cycles was characterized by FIB in Figure 4. In comparison with the film in Figure 2b, a relatively smooth surface morphology appears in Figure 4a, suggesting the composition of the SEI film may be changed after several electrochemical cycles. Furthermore, it is worthy to note that some holes with diameters of tens of nanometers (inset of Figure 4a) are formed on the film surface, indicative of gas production from electrolyte solution decomposition and subsequent releasing. As proposed by Aurbach et al.,[11,14] ethylene may be formed in accordance with the following equation: $2EC + 2e^- + 2Li^+ \rightarrow (CH_2OCO_2Li)_2\downarrow + CH_2 = CH_2\uparrow$. Therefore, it is reasonable to deduce that those electrolyte solutions diffused into cracks inside graphite spheres may also decompose and release gases, which will cause the increase of internal pressure and then the expansion of certain graphite spheres and the splitting of surface SEI films. The ELSA curves along the white line in the inset of Figure 4a are demonstrated in Figure 4c, where the contents of F, O, and P remain almost unchanged on the whole except for several valleys corresponding to the holes. But the content of C displays a gradual decrease along the line scanning direction. Aurbach et al.[15] pointed out that the surface films on the graphite electrode are formed by a highly selective process, i.e., the more reactive species react first. Hence, when the surface of the graphite sphere has been partly covered by the SEI film

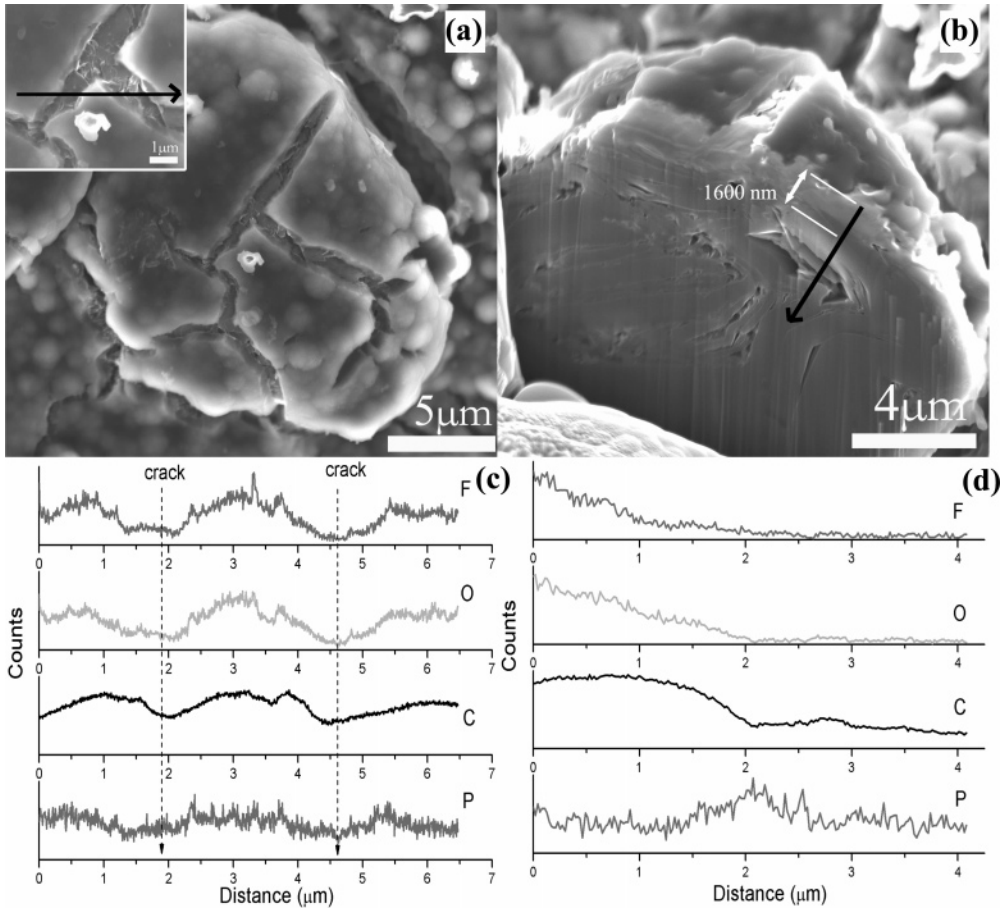

Figure 5. (a) A secondary electron FIB image of the natural graphite sphere after 24 discharge/charge cycles; the inset shows a magnified image. (b) The cross-section image of the graphite sphere. (c and d) The elemental line scan analysis along the black lines in panels a and b, respectively.

formed in the initial cycles, the decomposition of EC/DMC becomes selective on different surface parts; meanwhile, the reduction[11,16] of $LiPF_6$ ($LiPF_6 \leftrightarrow LiF\downarrow + PF_5$; $PF_5 + 2xLi^+ + 2xe^- \rightarrow Li_xPF_{5-x}\downarrow + xLiF\downarrow$; $PF_6 + 3Li^+ + 2e^- \rightarrow 3LiF\downarrow + PF_3$) is also restrained since it cannot contact with the graphite surface directly. In a word, based on the overall variations of F, O, C, and P (Figure 4c), it can be concluded that the content of organic compounds (CH_3OCO_2Li, $(CH_2OCO_2Li)_2$, CH_3OLi, etc.) increases in the SEI film and the surface composition is also non-uniform. The internal section of the natural graphite sphere and the associated ELSA curves along the white line are presented in Figure 4, panels b and d, respectively. On both sides of cracks A, B, and C, the "internal SEI film" can be obviously observed in terms of distinguishable contrast difference (Figure 4b); moreover, the ELSA results indicate the existence of F and O around the cracks, and their intensities of recorded counts are also similar to that of the freshly formed outer SEI film mentioned above, which further confirms the formation of the "internal SEI film". Compared with that in Figure 3b, the "internal SEI film" (Figure 4b) does not show an obvious growth, indicating that the "internal SEI film" is formed only at initial stages when the graphite sphere surface is not wrapped completely by the outer SEI film and electrolyte solutions can still penetrate into the internal cracks. Furthermore, it is also interesting to note that the content of phosphorus gives peaks at the cracks A, B, and C but fluorine gives valleys. This is because most of the decomposition products containing P (e.g., Li_xPF_y) only stay in the cracks and are not actively participating in the film formation, whereas most fluorides (e.g. LiF) contribute to the building of the SEI film.

Figure 5 shows the surface and internal microtexture of a natural graphite sphere after 24 discharge/charge cycles. In Figure 5a and the inset, several obvious cracks can be seen. This means that the SEI film splits upon repeated cycles due to the increase of internal pressure from gas (e.g., C_2H_2) production inside the sphere and the intercalation/deintercalation of Li^+ accompanied by volume change stress. Figure 5c shows the ELSA curves along the black line in the inset of Figure 5a. It is found that the variation tendencies of F, O, C, and P are similar: There are valleys and subsequent peaks around the cracks and the average content of each element remains nearly horizontal in the whole scanning range. Meanwhile, the cyclic efficiency at this electrochemical stage is ~100%, suggesting that the SEI film has been stable. Therefore, it is reasonable to conclude that the composition of the SEI film becomes uniform after reaching its stable state. Figure 5b presents the internal microtexture of the graphite sphere, where we can see that the outer SEI film thickens up to ~1600 nm. Moreover, we note again that the thickness of the "internal SEI film" does not increase obviously by comparing it with those in Figure 3b and Figure 4b. This indicates that once the "internal SEI film" is formed, it remains stable. Figure 5d shows the ELSA results along the black line in Figure 5b. According to the content variation tendency of each element, we can divide three segments from 0 to 1, 1 to 1.6, and 1.6 to 2 in the horizontal ordinate to correspond with the upper and bottom part of the outer SEI film and the "internal SEI film", respectively. In the range of 0 to 1, the ELSA curves of F and O show a gradual decrease, indicating that species such as LiF and Li_2O have a gradient distribution with the depth increment; as for C, its

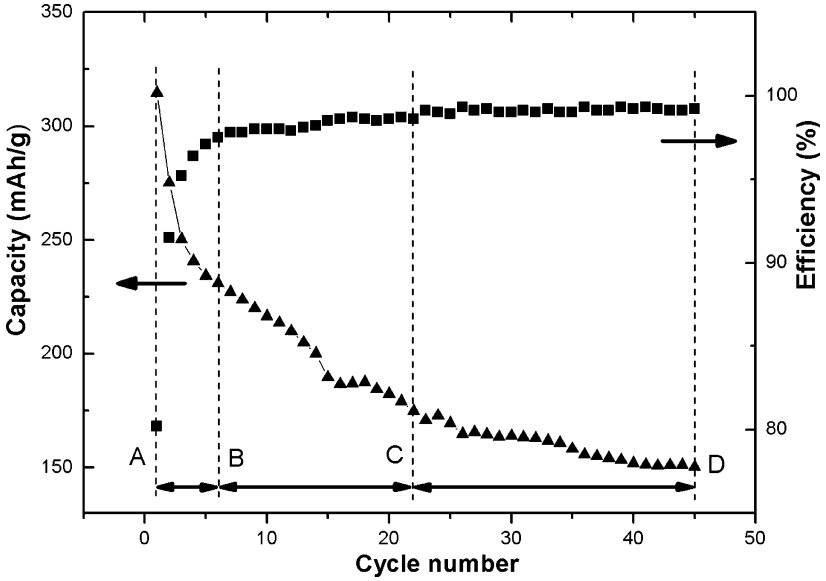

Figure 6. A typical plot of capacity and efficiency versus cycle number for natural graphite spheres galvanostatically charged/discharged in the voltage range of 0.001−2.5 V vs Li/Li$^+$ at a current density of 0.2 mA/cm^2 in an electrolyte of EC/DMC (1:1 volume ratio) with 1 M $LiPF_6$.

content remains nearly unchanged, which suggests that organic species from decomposition of EC/DMC may dominate this part. On the basis of these changes, it seems more likely that the SEI film is a mosaic of polyheteromicrophases as proposed by Peled et al.[4,5] In the range of 1 to 2, the content of F remains basically stable, but O and C decrease gradually. This is consistent with our former observations that there is a similar composition between the freshly formed outer SEI film and the "internal SEI film", in which fluorides such as LiF from the salt reduction predominate and organic compounds decrease gradually. In the whole range of 0 to 2, P gives a small peak just around the internal cracks, which is in agreement with our explanation above that phosphorus compounds incline to stay in the cracks and generally do not participate in the building of the SEI film.

A typical plot of capacity and efficiency versus cycle number for the natural graphite spheres is shown in Figure 6. On the basis of the above discussions on the formation and evolution of the SEI film, we propose capacity fading mechanisms of the natural graphite spheres. Three fractions (as demonstrated in Figure 6) can be divided according to the value of efficiency and the extent of sloping of the capacity curve. For the AB part where the capacity fades rapidly and the efficiency is lower than 96%, the main reason is due to the initial formation of the SEI film on the outer surface and the internal crack edge surface of the natural graphite spheres, which irreversibly consumes a large number of lithium ions. Especially during the formation of the "internal SEI film", many reversible Li$^+$ intercalation sites inside the graphite spheres are destroyed, and some gases are produced causing the increase of internal pressure that can lead to the exfoliation of graphite flakes. For the BC part where the efficiency is in the range of 96% to 98%, repeated splitting and repairing of the SEI film lead to an increase in film thickness and consequently in resistance. Meanwhile, the migration of lithium ions through the SEI film slows down. Therefore, the polarization of the electrode becomes severe, thus causing the capacity fading. For the CD part corresponding to the mild fading level of the capacity curve and the efficiency of nearly 100%, the SEI film has been basically stable. We speculate that the deactivation and structural degradation of certain natural graphite spheres wrapped by the SEI film, which gradually decrease reversible Li$^+$ sites, play a major role.

Conclusion

The initial SEI film with an apparent thickness range of ∼450 to ∼980 nm is rough in morphology and non-uniform in composition, containing small splits on the surface. After five electrochemical cycles, the SEI film with microscale holes becomes smooth and the content of the organic compounds increases. Obvious cracks can be seen on the SEI film after 24 discharge/charge cycles, and the thickness (∼1600 nm) also increases compared with that of the initial SEI film.

Furthermore, we demonstrated that a SEI film can also be formed around cracks inside the natural graphite spheres, and called it the "internal SEI film", which is relatively stable once formed. Its thickness does not increase obviously during cycling. We believe that the concept of "internal SEI film" is applicable not only for the natural graphite spheres specifically studied in this paper, but also for other anode materials with microcracks and micropores connecting their outer surface and inner part; further investigations are in progress.

On the basis of discussions of the evolution of the SEI film, we proposed the capacity fading mechanisms of the natural graphite spheres at three different electrochemical stages: first, the initial formation of the SEI film on the outer surface and internal crack edge surface; second, the splitting and repairing of the SEI film; and third, the deactivation and structural degradation of certain wrapped natural graphite spheres.

In a word, the results achieved in this study enrich the knowledge of the SEI film and may be helpful for the design and upgrading of high-performance lithium ion batteries.

Acknowledgment. This work was supported by the National Natural Science Foundation of China (No. 50328204) and the Hi-Tech Research and Development Program of MOST, China (No. 2002AA302401).

References and Notes

(1) Peled, E. *J. Electrochem. Soc.* **1979**, *126*, 2047.

(2) Peled, E.; Golodnitsky, D.; Aurbach, D.; Cohen, Y. S.; Wang, Z. X.; Huang, X. J.; Chen, L. Q.; Inaba, M.; Ogumi, Z.; Ploehn, H. J.; Ramadass, P.; White, R. E.; Altomare, D.; Sandi, G.; Edström, K.; Gustafsson, T.; Thomas, J. In *Lithium-Ion Batteries Solid−Electrolyte Interphase*; Balbuena, P. B.; Wang, Y. X., Eds.; Imperial College Press: London, UK, 2004.

(3) Peled, E.; Golodnitsky, D.; Penciner, J. In *Handbook of Battery Materials*; Besenhard, J. O., Ed.; Wiley-VCH: Weinheim, Germany, 1999; Chapter 6, p 419.
(4) Peled, E.; Golodnitsky, D.; Ardel, G. *J. Electrochem. Soc.* **1997**, *144*, L208.
(5) Peled, E.; Golodnitsky, D.; Ardel, G.; Eshkenazy, V. *Electrochim. Acta* **1995**, *40*, 2197.
(6) Peled, E.; Bar-Tow, D.; Merson, A.; Burstein, L. *J. New Mater. Electrochem. Syst.* **1999**, *3*, 21.
(7) Peled, E.; Bar-Tow, D.; Merson, A.; Gladkich, A.; Burstein, L.; Golodnitsky, D. *J. Power Sources* **2001**, *97*−*98*, 52.
(8) Peled, E.; Golodnitsky, D.; Ulus, A.; Yufit, V. *Electrochim. Acta* **2004**, *50*, 391.
(9) Aurbach, D.; Ein-Eli, Y.; Zaban, A. *J. Electrochem. Soc.* **1994**, *141*, L1.
(10) Aurbach, D.; Ein-Eli, Y. *J. Electrochem. Soc.* **1995**, *142*, 1746.
(11) Aurbach, D.; Markovsky, B.; Shechter, A.; Ein-Eli, Y. *J. Electrochem. Soc.* **1996**, *143*, 3809.
(12) Aurbach, D.; Weissman, I.; Yamin, H.; Elster, E. *J. Electrochem. Soc.* **1998**, *145*, 1421.
(13) Aurbach, D.; Markovsky, B.; Levi, M. D.; Levi, E.; Schechter, A.; Moshkovich, M.; Cohen, Y. *J. Power Sources* **1999**, *81*−*82*, 95.
(14) Aurbach, D.; Markovsky, B.; Weissman, I.; Levi, E.; Ein-Eli, Y. *Electrochim. Acta* **1999**, *45*, 67.
(15) Aurbach, D. *J. Power Sources* **2000**, *89*, 206.
(16) Aurbach, D.; Gnanaraj, J. S.; Levi, M. D.; Levi, E. A.; Fischer, J. E.; Claye, A. *J. Power Sources* **2001**, *97*−*98*, 92.
(17) Aurbach, D. *J. Power Sources* **2003**, *119*−*121*, 497.
(18) Levi, M. D.; Aurbach, D. *J. Phys. Chem. B* **1997**, *101*, 4630.
(19) Inaba, M.; Siroma, Z.; Kawatate, Y.; Funabiki, A.; Ogumi, Z. *J. Power Sources* **1997**, *68*, 221.
(20) Inaba, M.; Kawatate, Y.; Funabiki, A.; Jeong, S. K.; Abe, T.; Ogumi, Z. *Electrochim. Acta* **1999**, *45*, 99.
(21) Jeong, S. K.; Inaba, M.; Abe, T.; Ogumi, Z. *J. Electrochem. Soc.* **2001**, *148*, A989.
(22) Jeong, S. K.; Inaba, M.; Iriyama, Y.; Abe, T.; Ogumi, Z. *Electrochim. Acta* **2002**, *47*, 1975.
(23) Besenhard, J. O.; Winter, M.; Yang, J.; Biberacher, W. *J. Power Sources* **1995**, *54*, 228.
(24) Winter, M.; Wrodingg, G. H.; Besenhard, J. O.; Biberacher, W.; Novak, P. *J. Electrochem. Soc.* **2000**, *147*, 2427.
(25) Fong, R.; Sacken, U. V.; Dahn, J. R. *J. Electrochem. Soc.* **1990**, *137*, 2009.
(26) Herstedt, M.; Anderson, A. M.; Rensmo, H.; Siegbahn, H.; Eddtrom, K. *Electrochim. Acta* **2004**, *49*, 4939.
(27) Li, G. F.; Li, H.; Mo, Y. J.; Huang, X. J.; Chen, L. Q. *Chem. Phys. Lett.* **2000**, *330*, 249.
(28) Li, G. F.; Li, H.; Mo, Y. J.; Chen, L. Q.; Huang, X. J. *J. Power Sources* **2002**, *104*, 190.
(29) Balaya, P.; Li, H.; Kienle, L.; Maier, J. *Adv. Funct. Mater.* **2003**, *13*, 621.
(30) Dollé, M.; Grugeon, S.; Beaudoin, B.; Dupont, L.; Tarascon, J. M. *J. Power Sources* **2001**, *97*−*98*, 104.
(31) Tarascon, J. M.; Armand, M. *Nature* **2001**, *414*, 359.
(32) Cairney, J. M.; Munroe, P. R.; Hoffman, M. *Surf. Coat. Technol.* **2005**, *198*, 165.
(33) Liu, Y. L.; Jiao, C. *Solid State Ionics* **2005**, *176*, 435.
(34) Nakahara, S. *Surf. Coat. Technol.* **2003**, *169*−*170*, 721.
(35) Kong, F.; Kostecki, R.; Nadeau, G.; Song, X.; Zaghib, K.; Kinoshita, K.; McLarnon, F. *J. Power Sources* **2001**, *97*−*98*, 58.
(36) Yazami, R. *Electrochim. Acta* **1999**, *45*, 87.